Simulating the Aharonov-Bohm effect using the Crank-Nicolson Scheme

Dina Syverud-Lindland

Department of physics, Norwegian University of Science and Technology, 7034 Trondheim, Norway

Abstract

In this project, the Aharonov-Bohm effect is simulated numerically by solving the time-dependent Schrödinger equation with minimal coupling using the Crank-Nicolson scheme. A double-slit setup is used to analyze the phase shift induced by a confined magnetic flux, even for an electron in a region where the magnetic field is zero.

1. Introduction

The following implementation has been adapted from the works of Felix Deschroeters [4] and Benjamin Colmey [2]. The Crank-Nicolson (CN) scheme is used in an attempt to simulate the Aharonov-Bohm effect - a quantum phenomenon demonstrating the physical significance of electromagnetic potentials, even in regions where their respective electromagnetic fields are zero.

In the Aharonov-Bohm experiment, shown in Figure 1, an electron beam is split and directed around a solenoid containing a confined magnetic field. While the electrons traverse a region with zero magnetic field, they accumulate a relative phase shift, leading to a measurable interference pattern.

2. Theory

2.1. Minimal coupling

The wavefunction of a non-relativistic quantum system is governed by the Schrödinger equation (SE)

$$i\hbar\frac{d}{dt}\Psi = \hat{H}\Psi, \tag{SE}$$

where $\hat{H}$ is the Hamiltonian of the system.

The Lorentz force law states that the force of a particle with charge q is given by

$$\mathbf{F} = q(\mathbf{E} + \mathbf{v}\times\mathbf{B}), \tag{1}$$

where $\mathbf{E}$ and $\mathbf{B}$ are the electric and magnetic fields, respectively. Using that

$$\mathbf{E} = -\nabla\phi - \partial_t\mathbf{A} \quad \text{and} \tag{2}$$

$$\mathbf{B} = \nabla\times\mathbf{A}, \tag{3}$$

where ϕ is the electric potential and $\mathbf{A}$ is the magnetic vector potential. Inserting (2) and (3) into (1) yields the Hamiltonian

$$\hat{H} = \frac{1}{2m}(-i\hbar\nabla - q\mathbf{A})^2 + q\phi + V. \tag{4}$$

Here, V is an additional potential (like that of, e.g. a double slit). (4), combined with (SE) is known as the *minimal coupling rule* [3]:

$$i\hbar\frac{d}{dt}\Psi = \left[\frac{1}{2m}(-i\hbar\nabla - q\mathbf{A})^2 + q\phi + V\right]\Psi. \tag{5}$$

2.2. The Aharonov-Bohm effect

Consider a *gauge transformation*

$$V' = V - \partial_t\chi, \tag{6}$$

$$\mathbf{A}' = \mathbf{A} + \nabla\chi. \tag{7}$$

The *gauge structure* of Maxwell's theory says that any physical quantity should be invariant to any *gauge transformation*. However, in quantum mechanics, the fields play a more direct role. Note that $\Psi' = e^{iq\chi/\hbar}\Psi$ satisfies (5). The solution differs from Ψ by a phase factor, yet they represent the same physical state.

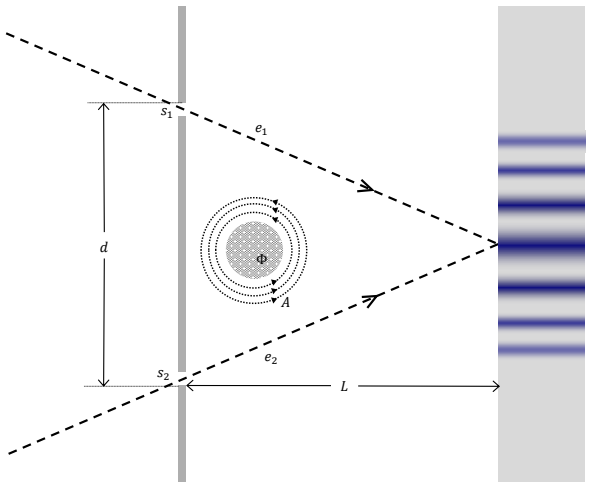

Figure 1: Schematic of the Aharonov-Bohm experiment. The electron beams interact with the double slit - a potential barrier with two slots, s_1 and s_2. There are two electron paths e_1 and e_2, and the phase of the wavefunction of electron(s) in e_1 are shifted with respect to that of electron(s) in e_2.

A physical consequence of this gauge invariance was demonstrated by physicists Yakir Aharonov and David Bohm in 1959 [7], when they showed that the vector potentials can affect the quantum-mechanical behavior of charged particles, even when confined to a region where **E** and **B** are zero.

Consider a particle of charge q moving in a region where $\mathbf{B} = \nabla \times \mathbf{A} = 0$, while $\mathbf{A} \neq 0$. Assume further that $\mathbf{A}$ is static. We can simplify the minimal coupling equation by writing

$$\Psi = e^{ig}\Psi',$$

where

$$g \equiv \frac{q}{\hbar}\int_{\mathcal{O}}^{\mathbf{r}} \mathbf{A}(\mathbf{r}') \cdot d\mathbf{r}' \tag{8}$$

with $\mathcal{O}$ being some arbitrarily chosen reference point. Note that the integral is independent of the path taken between the reference point and $\mathbf{r}$, because $\nabla \times \mathbf{A} = 0$. We have that

$$\nabla\Psi = e^{ig}(i\nabla g)\Psi' + e^{ig}(\nabla\Psi'). \tag{9}$$

However, $\nabla g = \frac{q}{\hbar}$, so we can write

$$(-i\hbar\nabla - q\mathbf{A})\Psi = -i\hbar e^{ig}\nabla\Psi', \tag{10}$$

$$\Rightarrow (-i\hbar\nabla - q\mathbf{A})^2\Psi = -\hbar^2 e^{ig}\nabla^2\Psi'. \tag{11}$$

Inserting this into (5) yields

$$-\frac{\hbar^2}{2m}\nabla^2 e^{ig}\Psi' = i\hbar\frac{\partial(e^{ig}\Psi')}{\partial t}. \tag{12}$$

So e^{ig} is just a phase factor correcting for the presence of the magnetic vector potential.

In the famous Aharonov-Bohm (solenoid) experiment, an electron beam is split in two, passing opposite sides of a long solenoid, as shown in Figure 1. The beams pass far enough away from the solenoid such that $\mathbf{B} = 0$. The magnetic vector field outside the solenoid, however, is *not* zero, "wrapping" around the solenoid:

$$\mathbf{A} = \frac{\Phi}{2\pi r}\hat{\phi} \quad \text{for} \quad r > R. \tag{13}$$

Here, R is the radius of the solenoid and Φ is the magnetic flux through the solenoid, given by $\Phi = \pi R^2 B = \pi R^2 \mu_0 n I$ (and I the current and n the coil density).

The electron beams each encounter a region with a vector potential in the opposite direction as that of the other one. When the beams arrive on the other side of the solenoid, they have different phases, given by

$$g = \frac{q}{\hbar}\int \mathbf{A}\cdot d\mathbf{r} = \frac{q}{\hbar}\int\left(\frac{\Phi}{2\pi r}\hat{\phi}\right)\cdot(r\hat{\phi}d\phi) = \pm\frac{q\Phi}{2\hbar}. \tag{14}$$

The sign indicates whether the passing electron is traveling in the *same* (+) or *opposite* (−) direction as $\mathbf{A}$.

As it turns out, the phase difference leads to measurable interference. The following section outlines how (5) can be solved numerically using the CN scheme to simulate the Aharonov-Bohm effect using a double slit potential.

2.3. Scaling of the differential equation

We can make (5) dimensionless by introducing the following parameters

$$\tau \equiv \frac{t}{t_c}, \quad \tilde{x} \equiv \frac{x}{l_c}, \qquad \tilde{y} \equiv \frac{y}{l_c} \quad \text{and} \quad \tilde{\mathbf{A}} \equiv \frac{\mathbf{A}}{A_c}, \tag{15}$$

where τ and x_c and y_c are natural length and timescales of the problem, defined by

$$t_c \equiv \frac{m}{A_c q}l_c, \quad l_c \equiv \frac{\hbar}{A_c q} \quad \text{with} \quad A_c \equiv \mu_0 I_0. \tag{16}$$

Considering the left-hand-side of (5), we see that

$$i\hbar\frac{d\Psi}{dt} = i\hbar\frac{t_c}{t_c}\frac{d\Psi}{dt} = i\hbar\frac{1}{t_c}\frac{d\Psi}{d\tau} = i\frac{A_c^2 q^2}{m}\frac{d\Psi}{d\tau}. \tag{17}$$

Similarly, for the first term in the parenthesis on the right-hand-side

$$\begin{aligned} -i\hbar\nabla &= -i\hbar\left(\frac{\partial}{\partial x}, \frac{\partial}{\partial y}\right) = -i\hbar\frac{1}{l_c}\left(\frac{\partial}{\partial\tilde{x}}, \frac{\partial}{\partial\tilde{y}}\right) \\ &= -iA_c q\tilde{\nabla}. \end{aligned} \tag{18}$$

Inserting the terms into (5), dividing by $m/A_c^2 q^2$ and setting $\phi = 0$ (this potential term will not be relevant in the following) the dimensionless minimal coupling rule now reads

$$i\frac{d\Psi}{d\tau} = \left[\frac{1}{2}(-i\tilde{\nabla} - \tilde{\mathbf{A}})^2 + \tilde{V}\right]\Psi = \tilde{H}\Psi, \tag{19}$$

where

$$\tilde{V} \equiv \frac{V}{V_c}, \quad \text{with} \quad V_c \equiv \hbar/t_c. \tag{20}$$

2.4. Solving the 2D SE with minimal coupling using the CN scheme

The CN method is an implicit, second-order time integration method that uses centered differences. (19) is approximated as:

$$i\frac{\Psi^{n+1} - \Psi^n}{\Delta\tau} = \frac{1}{2}\tilde{H}_{disc}(\Psi^{n+1} + \Psi^n), \tag{21}$$

where, $\tilde{H}_{disc}$ is the discretized dimensionless hamiltonian in (19). We see that the right-hand-side is an average between the backward and forward Euler methods. Collecting like terms, we obtain the CN matrix system

$$\begin{aligned} \left(I + \frac{i\Delta t}{2}\tilde{H}_{disc}\right)\Psi^{n+1} &= \left(I - \frac{i\Delta t}{2}\tilde{H}_{disc}\right)\Psi^n, \\ A\Psi^{n+1} &= M\Psi^n. \end{aligned} \tag{22}$$

To discretize $\tilde{H}$, we expand

$$\begin{aligned} \tilde{H} &= \frac{1}{2}\left[-\tilde{\nabla}^2 - i(\tilde{\mathbf{A}}\cdot\tilde{\nabla} + \tilde{\nabla}\cdot\tilde{\mathbf{A}}) + |\tilde{\mathbf{A}}|^2\right] + \tilde{V} \\ &= \frac{1}{2}\left[-\left(\frac{\partial^2}{\partial\tilde{x}^2} + \frac{\partial^2}{\partial\tilde{y}^2}\right) - i\left(\tilde{A}_x\frac{\partial}{\partial\tilde{x}} + \tilde{A}_y\frac{\partial}{\partial\tilde{y}}\right) + |\tilde{\mathbf{A}}|^2\right] \\ &\quad + V. \end{aligned} \tag{23}$$

In the last step we have used the *Coulomb gauge* ($\nabla \cdot \mathbf{A} = 0$) [5]. We consider the discretizations of the terms in (23). The Laplacian is discretized by combining [1]

$$\frac{\partial^2 \Psi}{\partial \tilde{x}^2} \approx \frac{\Psi_{i,j+1} - 2\Psi_{i,j} + \Psi_{i,j-1}}{(\Delta \tilde{x})^2},$$
$$\frac{\partial^2 \Psi}{\partial \tilde{y}^2} \approx \frac{\Psi_{i+1,j} - 2\Psi_{i,j} + \Psi_{i-1,j}}{(\Delta \tilde{y})^2}. \tag{24}$$

For simplicity, we hereon assume that $\Delta\tilde{x} = \Delta\tilde{y} \equiv \Delta l$. The discretized Laplacian term is thus

$$-\frac{1}{2}\tilde{\nabla}^2\Psi \approx -\frac{1}{2}\frac{\Psi_{i,j+1} + \Psi_{i,j-1} + \Psi_{i+1,j} + \Psi_{i-1,j} - 4\Psi_{i,j}}{(\Delta l)^2}. \tag{25}$$

In a similar manner, the momentum coupling term can be discretized

$$-\frac{i}{2}\left(\tilde{A}_x \frac{\partial}{\partial \tilde{x}} + \tilde{A}_y \frac{\partial}{\partial \tilde{y}}\right)\Psi$$
$$\approx -\frac{i}{2}\left(\tilde{A}_x \frac{\Psi_{i,j+1} - \Psi_{i,j-1}}{2\Delta l} + \tilde{A}_y \frac{\Psi_{i+1,j} - \Psi_{i-1,j}}{2\Delta l}\right). \tag{26}$$

Inserting (25), (26) and the respective $|\tilde{\mathbf{A}}|^2/2$ and $\tilde{V}$ terms into (21) and collecting like terms yields

$$\begin{aligned}
&\left\{i - 4\alpha - \Delta\tau\left[\frac{1}{2}(\tilde{A}_x^2 + \tilde{A}_y^2) - \tilde{V}\right]\right\}\Psi_{i,j}^{n+1} \\
&+\left\{\alpha + i\tilde{A}_x\beta\right\}\Psi_{i,j+1}^{n+1} + \left\{\alpha - i\tilde{A}_x\beta\right\}\Psi_{i,j-1}^{n+1} \\
&+\left\{\alpha + i\tilde{A}_y\beta\right\}\Psi_{i+1,j}^{n+1} + \left\{\alpha - i\tilde{A}_y\beta\right\}\Psi_{i-1,j}^{n+1} \\
&=\left\{i - 4\alpha - \Delta\tau\left[\frac{1}{2}(\tilde{A}_x^2 + \tilde{A}_y^2) - \tilde{V}\right]\right\}\Psi_{i,j}^{n} \\
&+\left\{-\alpha - i\tilde{A}_x\beta\right\}\Psi_{i,j+1}^{n} + \left\{-\alpha + i\tilde{A}_x\beta\right\}\Psi_{i,j-1}^{n} \\
&+\left\{-\alpha - i\tilde{A}_y\beta\right\}\Psi_{i+1,j}^{n} + \left\{-\alpha + i\tilde{A}_y\beta\right\}\Psi_{i-1,j}^{n}
\end{aligned} \tag{27}$$

where we have introduced the constants

$$\alpha \equiv \frac{\Delta\tau}{4(\Delta l)^2} \quad \text{and} \quad \beta \equiv \frac{\Delta\tau}{8\Delta l}. \tag{28}$$

This is the matrix system in (22), which can be solved using a numerical solver (e.g. spsolve, BiCGSTAB).

It's worth noting that because the CN scheme is numerically implicit, it is computationally expensive. However, when taking a look at (27), $\tilde{H}_{disc}$ takes a block-tri-diagonal form. One can therefore take great advantage of the use of sparse matrix storage formats, such as the *compressed sparse column* (CSC) format, which used in the code implementation.

[1] Note that, here, i-indices correspond to y-components, while j-indices correspond to x-components, as this is consistent with the structure of NumPy-arrays, which is used in the nummerical implementation.

3. Results

3.1. Double-slit diffraction for single electron

Figure 2 and Figure 3 displays single-electron diffraction at various timestamps[2].

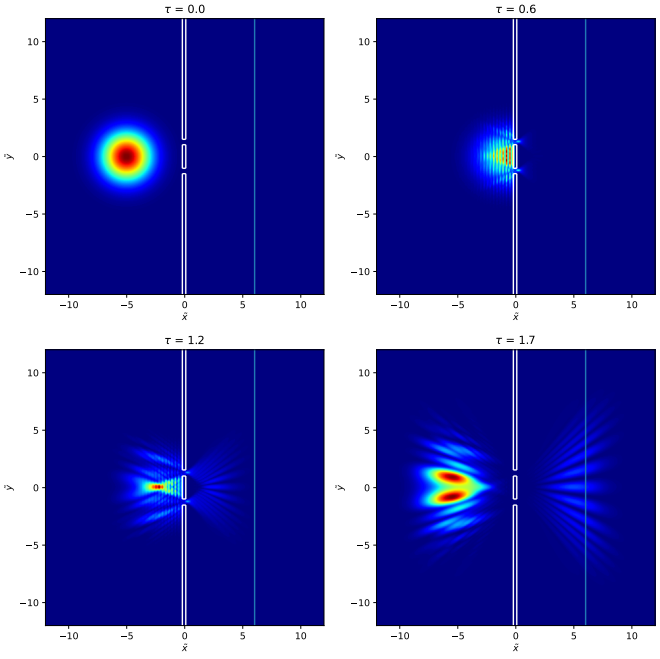

Figure 2: Two-dimensional probability density $|\Psi|^2$ of single electron at various time-steps τ of double-slit diffraction. The blue line indicates the "screen" at $\tilde{x} = 6.0$ where the diffraction pattern is measured in Figure 3.

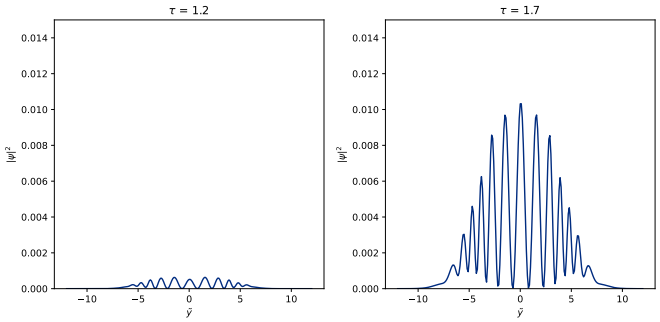

Figure 3: Cross-sectional (1D) probability density $|\Psi|^2$ of single electron at "screen" at $\tilde{x} = 6.0$ in Figure 2 and timesteps $\tau = 1.2$ and $\tau = 1.7$ of double-slit diffraction.

Figure 9 shows the distortion of the wavefunction over time. Some implications of this are discussed in subsection 4.1

[2] The code the code originally animated the simulation at each timestep. However, this is rather difficult to display in a paper.

3.2. Aharonov-Bohm effect

Figure 4 and Figure 5 show the control simulation where $\mathbf{A} = 0$. In Figure 6 and Figure 7, the a current has been turned on in the solenoid, creating an azimuthal vector potential. The vector potential is plotted in Figure 8.

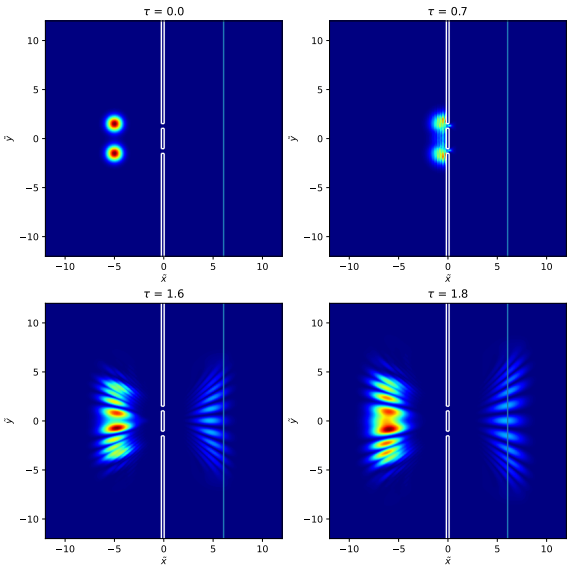

Figure 4: Two-dimensional probability density $|\Psi|^2$ of two electrons at various time-steps τ of the double-slit experiment (with $\mathbf{A} = 0$). The blue line indicates the "screen" at $\tilde{x} = 6.0$ where the diffraction pattern is measured in Figure 5.

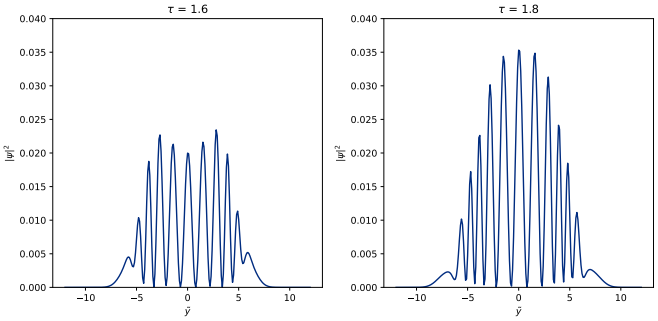

Figure 5: Cross-sectional (1D) probability density $|\Psi|^2$ of two electrons at $\tilde{x} = 6.0$ in Figure 4 and timesteps $\tau = 1.2$ and $\tau = 1.7$ in double-slit diffraction with $\mathbf{A} = 0$.

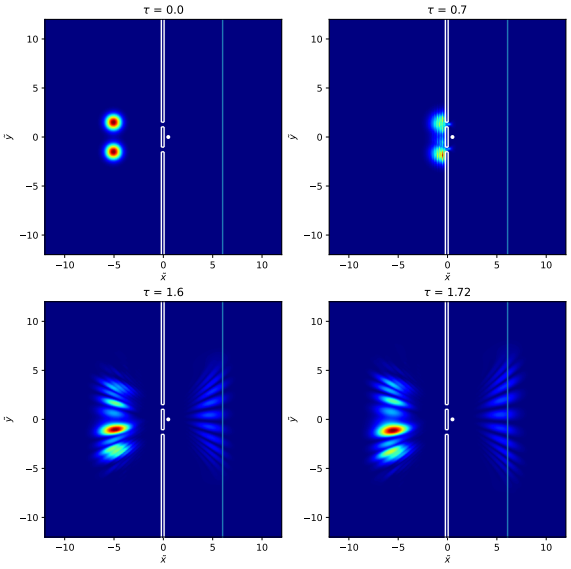

Figure 6: Two-dimensional probability density $|\Psi|^2$ of two electrons at various time-steps τ of double-slit diffraction with $\mathbf{A} \neq 0$. The blue line indicates the "screen" at $\tilde{x} = 6.0$ where the diffraction pattern is measured in Figure 7. The solenoid is indicated by a white dot.

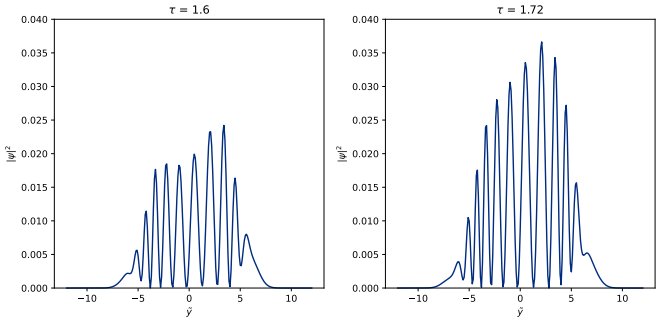

Figure 7: Cross-sectional (1D) probability density $|\Psi|^2$ of two electrons at $\tilde{x} = 6.0$ in Figure 6 and timesteps $\tau = 1.2$ and $\tau = 1.7$ in the double-slit experiment with $\mathbf{A} \neq 0$.

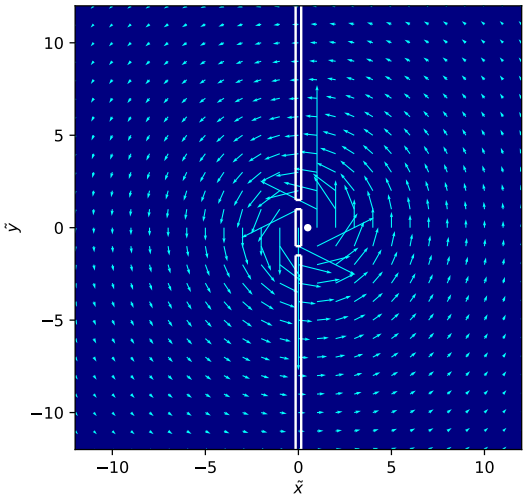

Figure 8: Magnetic vector potential $\mathbf{A}$ of a long solenoid given by (13) with $I = 10\,\mathrm{A}$.

4. Discussion

Figure 2 shows the probability density of a single electron traveling through a double slit. As expected, the wavefunctions traveling through each slit interfere with one another, producing the expected diffraction pattern on the "screen". This exhibits the *wave-particle duality* of electrons.

Figure 4 and Figure 5 display double-slit diffraction for two electrons (with $\mathbf{A} = 0$). In essence, the effect is the same as that of the single electron, and the same diffraction pattern is observed at the screen, only more pronounced. The left graph in Figure 5 shows a dip in the middle peaks at $\tau = 1.6$. This is because the two electrons have initial positions centered around different $\tilde{y}$-positions.

Figure 6 shows the Aharonov-Bohm effect. As the wavefunctions interact with the magnetic vector potential, a phase shift occurs. The phase shift is observed by comparing Figure 7 and Figure 5, clearly exhibiting a difference in the interference pattern under the influence of $\mathbf{A}$.

Aharonov and Bohm 1959 wrote in 1959 that "In principle, we could do the experiment with and without the magnetic flux. But since the main effect of the flux is only to displace the line pattern without changing the interval structure, this would not be a convenient experiment to do" [7]. As seen by comparing Figure 5 and Figure 7, one can see that the peak has been shifted, as expected. However, one also sees that there indeed *is* a change to the interval structure. This could suggest some problems with the model.

Further, it is suggested to rather "vary the magnetic flux within the same exposure for the detection of the interference pattern" which could "alter the sharpness and the general form of the interference bands" [7]. An extension of the simulation could be to model electron *beams* rather than single electrons, and varying the A-field rapidly over time, as suggested. However, altering the magnetic field would induce an electric field outside the solenoid, which by (1), would act on the wavefunction and possibly be problematic.

4.1. Limitations of the numerical method

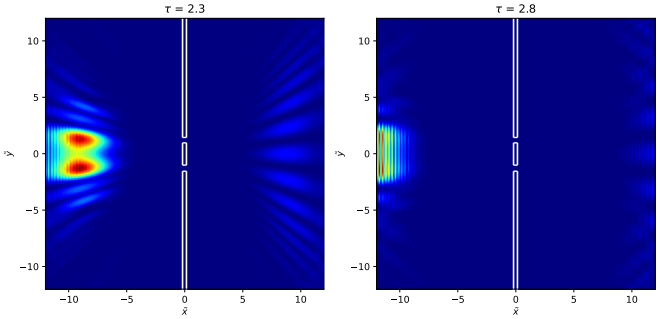

Figure 9: Wavefunction Ψ reflected at boundaries as the simulation progresses.

Numerically solving the heat equation for a wavefunction defined on an *infinite* domain is inherently difficult, as the computation is done on a *finite* grid. This requires imposing artificial boundary conditions. The structure of (22) and (27) implicitly enforces Dirichlet boundary conditions at the edges of the grid, because Ψ cannot interact with points outside the grid, essentially making it zero at the boundaries. This causes an *unphysical* reflection of the wave, shown in Figure 9.

The time interval and region of interest of the simulation did not involve reflections. However, in order to improve the simulation with regards to this problem, *perfectly matched layers* (PMLs) could be implemented. These are artificial "absorbing" layers, that absorb any unphysical reflection by damping the wave at the boundary of the truncated region, such that it exponentially decays [1].

5. Conclusion

This project presents a numerical simulation of the Aharonov-Bohm effect using the CN scheme to solve the minimal coupling rule. The results demonstrate that the presence of a vector potential induces a phase shift in electron wavefunctions, even in regions where the magnetic field is absent. The interference pattern observed in the double-slit experiment exhibits a phase shift, in accordance with the fundamental predictions of the Aharonov and Bohm.

It should be noted that the implementation makes many assumptions and is a simplification of the original experiment. However, with the success of the CN-scheme in solving the SE, this model has some *potential*.

References

[1] Jean-Pierre Beregner. A perfectly matched layer for the absorption of electromagnetic waves. *Jounal of Computational Physics*, 114(2):185–200, 1994. DOI: https://doi.org/10.1006/jcph.1994.1159.

[2] Benjamin Colmey. *Aharonov-Bohm-Space-Charge-Effects-in-Python*, GitHub, 2023. https://github.com/bcolmey/Aharonov-Bohm-Space-Charge-Effects-in-Python. Last accessed: 10.03.2025.

[3] David J. Griffiths and Darrell F. Schroeter. *Introduction to Quantum Mechanics*. Cambridge University Press, 3rd edition, 2018.

[4] Felix Deschroeters. *Electron-diffraction*, GitHub, 2019. https://github.com/FelixDesrochers/Electron-diffraction. Last accessed: 10.03.2025.

[5] David J. Griffiths. *Introduction to Electrodynamics*. Cambridge University Press, 5th edition, 2023.

[6] Hans P. Langtangen and Geir K. Pedersen. *Scaling of Differential Equations*. SpringerOpen, 2016.

[7] Yakir Aharonov and David Bohm. Significance of electromagnetic potentials in the quantum theory. *Physical Review*, 115(3):485–491, 1959. DOI: https://doi.org/10.1103/PhysRev.115.485.